

This section contains shorter technical papers. These shorter papers will be subjected to the same review process as that for full papers.

Scuffing Failure of Hydrodynamic Bearings Due to an Abrasive Contaminant Partially Penetrated in the Bearing Over-Layer

Mircea D. Pascovici

Professor and Head, Department of Machine Elements and Tribology, Polytechnic University of Bucharest, Bucharest, 79590, Romania

M. M. Khonsari

Dow Chemical Endowed Chair and Professor, Department of Mechanical Engineering, Louisiana State University, Baton Rouge, LA 70803
e-mail: e-mail: khonsari@me.lsu.edu

1 Introduction

Recently Khonsari et al. [1] analyzed the scuffing failure of hydrodynamic bearings caused by an abrasive contaminant. Modeled as a spherically shaped rigid particle, the contaminant was envisioned to penetrate into the protective over-layer while positioning itself in rubbing contact with the slider. Excessive temperature rise between the particle-slider interface was used as an indication of whether scuffing would take place. The model uses this temperature rise in conjunction with the material properties to determine the critical particle size that may result in scuffing failure. This information can be used as a guide for selecting an appropriate filter size. The tendency over the past decade or so has been to utilize finer filter sizes to enhance components' lifetimes by reducing wear associated with abrasive contamination (see Fisher and Donahue [2]). However, an ultra-fine filter is susceptible to clogging and therefore requires frequent attention.

Analysis shows that the depth of the particle penetration in the over-layer, δ , is an important parameter of the model (cf. Khonsari et al. [1]). Depending on the penetration depth, three distinct situations are envisioned:

1 A particle may fully penetrate into the over-layer (i.e., $\delta_2 \geq D$) thus embedding itself fully in the bearing liner.

2 Alternatively, a particle's penetration depth may be greater than that of the particle's radius but smaller than that of the particle diameter ($D/2 \leq \delta_2 \leq D$). This so-called "diametric penetration," is perhaps most representative of relatively larger particles in bearings which operate under moderate operating speeds.

3 When the abrasive particle is relatively small and the oper-

ating speed is large, there is a possibility that a particle may find itself in a so-called "partially penetration" position where $\delta_2 \leq D/2$ (Fig. 1).

The first situation is least hazardous as far as scuffing is concerned. The second case was treated in the paper by Khonsari et al. [1]. In the present paper, we shall focus our attention to the partial penetration (case 3). Examples are provided to illustrate the utility of the model in determining an appropriate filter size, which could reduce the chance of scuffing failure.

2 Model

Consider a particle in a partially embedded position as shown in Fig. 1. The contact temperature at the slider-particle interface is a function of the mean fluid temperature, T , and the flash temperature, T_f . The flash temperature is a function of the friction coefficient, size of the contact, the load, the velocity, and the thermo-mechanical properties of the material.

2.1 Penetration Depths. Let a_1 and a_2 represent the contact radii at the particle-slider and particle-liner, respectively. Assuming that the shaft surface is smooth, the load carried by a single particle is

$$W_p = 0.5\pi a_2^2 \sigma_2 = 0.5\pi a_1^2 \sigma_1, \quad (1)$$

where σ_1 and σ_2 represent the hardness of the slider and the over-layer, respectively. The parameter β denotes the hardness ratio, $\sigma_1 = \beta\sigma_2$.

From equation (1), it can be deduced that

$$a_2^2 = \beta a_1^2. \quad (2)$$

The geometric constraint between the penetration depths and the minimum film thickness is

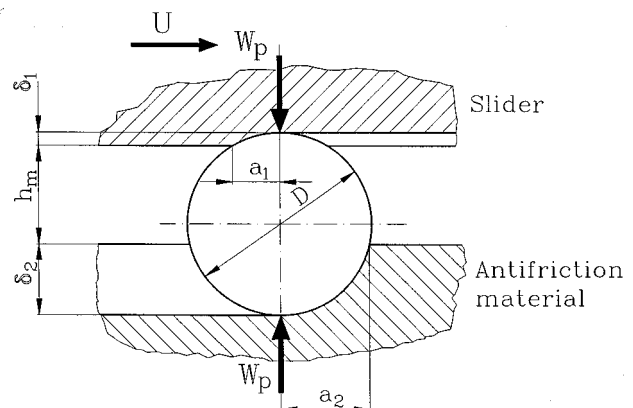


Fig. 1 Schematic of a partially penetrated particle in the anti-friction material

Contributed by the Tribology Division for publication in the ASME JOURNAL OF TRIBOLOGY. Manuscript received by the Tribology Division March 14, 2000; revised manuscript received June 29, 2000. Associate Editor: T. C. Ovaert.

$$D = \delta_1 + \delta_2 + h_m. \quad (3)$$

The geometry of contact provides the following relationship:

$$a_i^2 = D \delta_i - \delta_i^2, \quad (4)$$

where the subscripts, $i = 1, 2$ refer to the slider and the over-layer, respectively.

The penetration depth δ_1 can be put in terms of the hardness ratio, β , using Eqs. (2) and (4). The result is

$$\delta_1^2 - D \delta_1 + a_2^2 / \beta = 0. \quad (5)$$

Combining Eqs. (3) and (4) we obtain

$$a_2^2 = D h_m + D \delta_1 - h_m^2 - \delta_1^2 - 2 h_m \delta_1. \quad (6)$$

Substituting (6) into (5) and solving for the penetration depth yields

$$\bar{\delta}_1 = \frac{\beta - 1 + 2 \bar{h}_m - \sqrt{(\beta - 1 + 2 \bar{h}_m)^2 - 4 \bar{h}_m (1 - \bar{h}_m) (\beta - 1)}}{2 (\beta - 1)}, \quad (7)$$

where $\bar{\delta}_1 = \delta_1 / D$ and $\bar{h}_m = h_m / D$.

The obvious singularity in Eq. (7) when $\beta = 1$ can be treated by the application of the L'Hospital's rule. The result is

$$\bar{\delta}_1 = (1 - \bar{h}_m) / 2. \quad (8)$$

In the case of a partial penetration, $\bar{\delta}_2 < 0.5$ and the dimensionless minimum film thickness must be higher than a limiting value \bar{h}_m^* (when $\bar{\delta}_2 = 0.5$). This value will be obtained from Eqs. (2), (3), and (4). Therefore, when $\bar{\delta}_2 = 0.5$, Eq. (2) dictates that

$$\frac{D^2}{4} = \beta a_1^2. \quad (9)$$

Eliminating a_1 between Eqs. (4) and (9) and equating the dimensionless penetration $\bar{\delta}_1$ is

$$\bar{\delta}_1 = 0.5 (1 - \sqrt{1 - 1/\beta}). \quad (10)$$

The limiting value of \bar{h}_m^* is obtained by eliminating $\bar{\delta}_1$ between Eqs. (3) and (10). The result is

$$\bar{h}_m^* = 0.5 \sqrt{1 - 1/\beta}. \quad (11)$$

2.2 Coefficient of Friction. The friction coefficient, f , between the particle and the slider is governed by two mechanisms: plowing f_p and adhesion f_a . The plowing component is simply the product between the slider hardness σ_1 and the area of a sector-shaped groove at the particle-shaft interface [3]. The adhesion component is obtained by integration of the shear stress, τ , which is assumed to be uniform over the entire hemispherical area of contact (cf. Komvopoulos [4]). For a particle configuration shown in Fig. 1, the friction coefficient is:

$$f = \frac{\cos^{-1}(1 - 2 \bar{\delta}_1) - 2(1 - 2 \bar{\delta}_1) \sqrt{\bar{\delta}_1 - \bar{\delta}_1^2} + 4 \bar{\tau}_1 \bar{\delta}_1}{2 \pi (\bar{\delta}_1 - \bar{\delta}_1^2)}, \quad (12)$$

where $\bar{\tau}_1$ is the shear stress at the slider-particle interface. Equation (12) can be simplified for rapid calculation of friction coefficient as

$$f \cong \frac{1}{\pi} \left(\frac{8 \sqrt{\bar{\delta}_1}}{3(1 - 2 \bar{\delta}_1)} + 2 \bar{\tau}_1 \right). \quad (13)$$

This approximate expression is valid for partial penetrations of $\bar{\delta}_1 < 0.1$. The error associated with Eq. (13) is less than 1.5 percent for $\bar{\delta}_1 \leq 0.03$.

The shear stress component $\bar{\tau}_1$ is related to the penetration depth at the slider-particle interface. According to the experimental and theoretical studies published by Hokkirigawa and Kato [5],

Johnson [6], Kato [7], Lim [8], and Zum Gahr [9] the plowing mode of friction exists only if the penetration $\bar{\delta}_1$ is small enough. When plowing mode of friction dominates, a "zero degree of wear" for the shaft surface will be expected. For small penetration depths of $\bar{\delta}_{1,p} \leq 0.04$, the following relationship is proposed:

$$\bar{\tau}_1 = 2.5 \bar{\delta}_1 / \sqrt{\bar{\delta}_1 - \bar{\delta}_1^2} \quad (14)$$

2.3 Average Flash Temperature. The average flash temperature at the particle-slider interface can be determined using the following expression (cf. Tian and Kennedy [10]; Khonsari et al. [1]):

$$T_f = \frac{\lambda f W_p U}{3.701 K a_1^*}, \quad (15)$$

where $K = k_1 / k_p$ (the ratio of the slider thermal conductivity over that of the particle); $a_1^* = (D \sqrt{2}/2) \sqrt{\bar{\delta}_1 - \bar{\delta}_1^2}$ (the equivalent contact radius); and $\lambda = (1 + K \sqrt{1 + 0.537 \text{Pe}_D \sqrt{\bar{\delta}_1 - \bar{\delta}_1^2}})^{-1}$, representing the heat partitioning factor between the slider and the particle. This parameter is a function of the Peclet number defined below

$$\text{Pe}_D = \frac{UD}{\alpha_1}, \quad (16)$$

where α_1 is the thermal diffusivity of the slider.

For the case of partial penetration, the appropriate expression for the flash temperature in dimensionless form is

$$\bar{T}_f = \frac{0.191 \pi K \text{Pe}_D f \sqrt{\bar{\delta}_1 - \bar{\delta}_1^2}}{1 + K \sqrt{1 + 0.537 \text{Pe}_D \sqrt{\bar{\delta}_1 - \bar{\delta}_1^2}}}, \quad (17)$$

where $\bar{T}_f = T_f K / (\sigma_1 \alpha_1)$.

3 Level of Filtration

Having obtained appropriate expressions for the flash temperature in terms of the parameters of the particle, shaft and the over-layer, we are now in the position to determine the necessary level of filtration. Scuffing failure is assumed to occur when the flash temperature exceeds a certain critical value, T_{cr} . In this model, the critical flash temperature is depended upon several key parameters. They are (1) minimum film thickness h_{min} , which is governed by the bearing operating conditions such as speed, load, and the type of lubricant and the inlet supply temperature; (2) particle type, characterized in terms of its thermal conductivity; (3) type of bearing over-layer, characterized by the hardness ratio, β ; and (4) shaft speed, U . For a given speed, the proper level of filtration is one which allows through passage of the particles smaller than or equal to the critical size, D_{cr} . In other words, a particle whose size is equal to or greater than D_{cr} can produce a flash temperature greater than the critical flash temperature, thus leading to scuffing failure.

The dimensionless critical flash temperature is

$$\bar{T}_{fcr} = \bar{T}_{cr} - \bar{T}. \quad (18)$$

Once the critical Peclet number is known, an appropriate filter size must be selected such that

$$\text{Pe}_D \leq \text{Pe}_{Dcr} \quad (19)$$

or equivalently,

$$D \leq D_{cr}.$$

The critical Peclet number can be conveniently expressed in terms of the dimensionless flash temperature as follows:

$$Pe_{D_{cr}} = \chi + 0.2685K^2\chi^2\sqrt{\bar{\delta}_1 - \bar{\delta}_1^2} + \sqrt{(\chi + 0.2685K^2\chi^2\sqrt{\bar{\delta}_1 - \bar{\delta}_1^2})^2 + \chi^2(K^2 - 1)}, \quad (20)$$

where $\chi = (5.235\bar{T}_{fcr}) / (\pi K f \sqrt{\bar{\delta}_1 - \bar{\delta}_1^2})$.

Examination of the above equations shows that the higher the Peclet number (or the operating speed), the higher the flash temperature. Also, the smaller the minimum film thickness, the higher the flash temperature. Hence, from scuffing point of view, the higher the flash temperature, the greater likelihood of failure. Also worth noting is that when the hardness ratio β is small, the particle penetration is less. Therefore, for a given minimum film thickness and Peclet number, a greater flash temperature is expected with an over-layer whose yield stress is large. For example, a four-fold increase in β results in a roughly two-fold reduction of the flash temperature.

4 Application

Example 1. Consider a journal bearing with a babbitted sleeve and steel shaft of diameter $D = 100$ mm operating at $U = 6.4$ m/s with a minimum film thickness of $h_{\min} = 25$ μ m. Assume that the bearing mean temperature is $T = 60^\circ\text{C}$. The bearing material specifications are as follows:

For a babbit over-layer, the hardness ratio is $\beta_2 = 16$ and the critical temperature is $T_{cr} = 150^\circ\text{C}$. The shaft hardness value is: $\sigma_1 = 1700$ MPa. The shaft thermal diffusivity and thermal conductivity are $\alpha_1 = 13 \times 10^{-6}$ m²/s and $k_1 = 45$ W/mK, respectively.

Case 1. Determine the adequacy of a 40 μ m filter size if the bushing over-layer is made of babbit.

First it must be established whether the partial embedability condition is satisfied. Using Eq. (11), the dimensionless film thickness is

$$\bar{h}_m^* = 0.5\sqrt{1 - 1/\beta} = 0.5\sqrt{1 - 1/16} = 0.484.$$

Since $\bar{h}_m^* < 0.5$, the partial embedability condition is satisfied.

The deformation at the particle-shaft interface is predicted from Eq. (7):

$$\bar{\delta}_1 = \frac{15 + 2\bar{h}_m - \sqrt{(15 + 2\bar{h}_m)^2 - 60\bar{h}_m(1 - \bar{h}_m)}}{30} = 0.0146 < \bar{\delta}_{1p}$$

which in dimensional form is: $\delta_1 = 0.0146 \times 40 = 0.585$ μ m.

Friction coefficient is

$$f = \frac{1}{\pi} \left(\frac{8\sqrt{\bar{\delta}_1}}{3(1 - \bar{\delta}_1)} + \frac{5\bar{\delta}_1}{\sqrt{\bar{\delta}_1 - \bar{\delta}_1^2}} \right) = 0.304.$$

The Peclet number is

$$Pe_D = UD_{cr} / \alpha_1 = 19.7.$$

For a steel particle, $K = 1$ and using Eq. (17), the dimensionless flash temperature is predicted to be:

$$\bar{T}_f = \frac{0.191\pi K Pe_D f \sqrt{\bar{\delta}_1 - \bar{\delta}_1^2}}{1 + K\sqrt{1 + 0.537 Pe_D \sqrt{\bar{\delta}_1 - \bar{\delta}_1^2}}} = 0.169$$

which translates to a temperature rise of 83 K. Therefore, the critical temperature becomes

$$T_{cr} = T + T_f = 60 + 83 = 143^\circ\text{C}.$$

This temperature is lower than the critical flash temperature associated with the babbit which is taken to be $T_{crf} = 150^\circ\text{C}$. Therefore, the filter size of 40 μ m is adequate and according to the model presented there is no danger of scuffing failure.

Case 2. Determine if the 40 μ m filter is adequate if the particulate matter were made of Silicon dioxide, i.e., sand, which possesses much lower thermal conductivity than steel. The ratio of the thermal conductivity of steel to that of SiO₂ is: $K = 9.57$. Repeating the calculations, we obtain, $\bar{T}_f = 0.282$ which in dimensional form predicts a temperature rise of $T_f = 138$ K. Therefore, the critical temperature rise in this case is

$$T_{cr} = T + T_f = 60 + 138 = 198^\circ\text{C}.$$

This temperature is much greater than $T_{crf} = 150^\circ\text{C}$ and scuffing is likely to occur. Therefore, it follows that the filter size is inadequate if this bearing is to function in a dusty environment.

Case 3. Determine if a 30 μ m filter could provide adequate protection for this bearing in the presence of sand particles.

Repeating the above procedure, we obtain that $\bar{T}_f = 0.0172$ which translates to a temperature rise of $T_f = 84$ K. Therefore, the critical temperature rise in this case is:

$$T_{cr} = T + T_f = 60 + 84 = 144^\circ\text{C}$$

which is below the critical flash temperature of 150°C and is indicative of the filter adequacy even in the dusty environment.

Example 2. Consider now the same operating condition as in example 1. However, let us assume that the bushing over-layer is made of bronze. For a bushing with bronze over-layer, a greater shaft hardness is generally chosen [11,12]. For this reason, we take $\sigma_1 = 3000$ MPa. The associated hardness ratio and the critical temperature are:

$$\beta_1 = 5; \quad T_{cr} = 230^\circ\text{C}.$$

We will examine the appropriateness of a 30 μ m assuming that particulate matter is made of steel.

Similar calculations as illustrated in example 1 show that $\bar{T}_f = 0.217$, $T_f = 188$ K, and the critical temperature is $T_{cr} = T + T_f = 60 + 188 = 248^\circ\text{C}$ which is greater than the allowable maximum temperature of 230°C . Therefore this filter is inadequate for protecting the bearing against steel particles and/or sand particles. This conclusion is supported by a recent paper by Duchowski [13] who recommends filter elements rated at 6 μ m. While one may seek to utilize a finer filter size for this application, it must be born in mind that a very fine filter size requires frequent attention to avoid complete blockage of the lubricant passage due to clogging. An ultra-fine filter also has the disadvantage of causing excessive power loss due to large pressure drop across the filter.

Concluding Remarks

In a companion article, Khonsari et al. [1] established a relationship between scuffing failure and particulate contamination due to an abrasive particle which bridges itself across the gap between the protective over-layer and the sliding surface. Entire set of governing equations and results were presented by assuming that the particle penetration depth was greater than the particle radius. The term diametric penetration was used to characterize the depth of particle penetration situation. In this paper, the governing equations are extended to the "partially penetrated" situations where the particle penetration depth is much less than the particles' radius. The formulations presented in this paper best represent the situations where particle size is relatively small and/or the operating speed is large. The governing equations enable one to readily determine an appropriate filter size for a given set of bearing specifications and operating conditions. A series of examples are presented to illustrate the utility of the results.

It should be mentioned that analytical treatment of particulate contamination problems in hydrodynamic bearings is indeed complicated because of the large number of interrelated parameters that are involved. Several simplifying assumptions had to be made in order to arrive at a practical set of governing equations that can be utilized at the design stage. Current bearing design practice

relies heavily on the allowable minimum film thickness based on the surface finish and the specified operating conditions without consideration of the appropriate filter size. Further research is therefore needed to relate the bearing parameters with thermohydrodynamic analysis, particularly with consideration of the bearing and shaft surface roughness. The present paper and its companion article by Khonsari et al. [1] represent a first step toward fulfillment of this need.

Acknowledgment

This research was sponsored in part by the National Research Council. The authors gratefully acknowledge the financial support and encouragement of the program director, Ms. Kelly Robbins, throughout the course of this investigation.

References

- [1] Khonsari, M., Pascovici, M., and Kuchinschi, B., 1999, "On the Scuffing Failure of Hydrodynamic Bearings in the Presence of an Abrasive Contaminant," *ASME J. Tribol.*, **121**, pp. 90–96.
- [2] Fisher, G., and Donahue, A., 2000, "Filter Debris Analysis as a First-Line Condition Monitoring Tool," *Lubr. Eng.*, **56**, pp. 18–22.
- [3] Moore, D. F., 1975, *Principles and Applications of Tribology*, Pergamon Press, Oxford.
- [4] Komvopoulos, K., 1991, "Sliding Friction Mechanisms of Boundary-Lubricated Layered Surfaces: Part II—Theoretical Analysis," *Tribol. Trans.*, **34**, pp. 281–291.
- [5] Hokkirigawa, K., and Kato, K., 1988, "Experimental and Theoretical Investigation of Ploughing, Cutting and Wedge Formation During Abrasive Wear," *Tribol. Int.*, **21**, No.1, pp. 51–57.
- [6] Johnson, K. L., 1995, "Contact Mechanics and the Wear of Metals," *Wear*, **150**, pp. 162–170.
- [7] Kato, K., 1997, "Wear Mechanism," *New Directions in Tribology*, Mechanical Engineering Publications (M.E.P.) Ltd., pp. 39–56.
- [8] Lim, S. C., 1997, "Recent Developments in Wear-Mechanism Maps," *New Directions in Tribology*, Mechanical Engineering Publications (M.E.P.) Ltd., pp. 309–320.
- [9] Zum Gahr, K.-H., 1997, "Wear by Hard Particles," *New Directions in Tribology*, Mechanical Engineering Publications (M.E.P.) Ltd., pp. 483–494.
- [10] Tian, X., and Kennedy, F. E., 1994, "Maximum and Average Flash Temperatures in Sliding Contacts," *ASME J. Tribol.*, **116**, pp. 167–174.
- [11] Anonymous, 1989, "Mechanical Systems. Bearings and Lubricants," *Machine Design* (Power and Motion Control Reference Volume), **61**, No. 12, pp. 324–325.
- [12] Schilling, A., et al., 1972, *Automobile Engine Lubrication*, Vol. II, Scientific Publications Ltd.
- [13] Duchowski, J. K., 1998, "Examination of Journal Bearing Filtration Requirements," *Lubr. Eng.*, **54**, pp. 18–28.

The Variation of Viscosity With Temperature and Pressure for Various Real Lubricants

Scott Bair

Principal Research Engineer, George W. Woodruff School of Mechanical Engineering, Georgia Institute of Technology, Atlanta, GA 30332

To date, nearly all analyses of lubricant traction behavior in the Hertzian zone of concentrated contact have been performed with viscosity correlations which understate the effect of pressure and temperature at high pressures. We present viscometer measurements of lubricant viscosity for pressures to 1.4 GPa and tem-

peratures to 165°C for various lubricants including automotive transmission fluids, aerospace lubricants, a turbine oil, and a metal working oil. Parameters of a free-volume correlation are provided for use in numerical modeling of traction, film thickness, and roughness interactions in concentrated contact.
[DOI: 10.1115/1.1308024]

1 Introduction

Viscosity is clearly the most important property of a concentrated contact lubricant. The analysis of traction and micro-EHD requires a relationship between viscosity and temperature and pressure. Although measurements of viscosity to pressures of several gigapascal have been available in the physics literature for 50 years [1], many tribologists have simply assumed a viscosity relation that provides agreement between experiment and the assumed constitutive behavior. These assumed pressure-temperature-viscosity relations have underestimated the pressure-viscosity coefficient at high pressures [2,3]. We show that the temperature-viscosity coefficient is underestimated as well. Then clearly a need exists for temperature-pressure-viscosity correlations for real liquid lubricants.

We present viscometer measurements of lubricant viscosity to pressures to 1.4 GPa and temperatures to 165°C for various lubricants, including automotive transmission fluids, aerospace lubricants, a turbine oil and a metal working oil. Parameters of a free-volume correlation are provided for use in numerical modeling of traction, film thickness and roughness interactions in concentrated contact.

2 Temperature-Viscosity Effects at High Pressure

It has long been appreciated that for a representation of viscosity in the high-packing density regime, an important parameter is the temperature at which the viscosity $\mu \rightarrow \infty$ [4]. This parameter appears explicitly in the Vogel equation and the Williams, Landel, and Ferry equation. However, for analyses involving both thermal and piezoviscous effects in concentrated contact lubrication, tribologists have typically represented the viscosity by the Roelands [5] equation,

$$\mu = \mu_0 \exp \left\{ \ln \left(\frac{\mu_0}{\mu_r} \right) \left[\left(1 + \frac{p}{p_r} \right)^z \left(\frac{T_0 + 135^\circ\text{C}}{T + 135^\circ\text{C}} \right)^s - 1 \right] \right\} \quad (1)$$

Here, p_r and μ_r are a reference pressure and viscosity and T_0 is the temperature at which the viscosity is μ_0 at pressure, $p = 0$. The dimensionless pressure index is z and the temperature index is s . Note that $\mu \rightarrow \infty$ for $T = -135^\circ\text{C}$ regardless of pressure. The behavior is intuitively unreasonable since it is known that the glass transition temperature, which is typically 30°C to 80°C greater than the temperature at the viscosity singularity, is known to increase significantly with pressure. Indeed, free volume arguments predict that for any temperature there must be a pressure [6] at which $\mu \rightarrow \infty$. Actually, one does not encounter the unbounded viscosity with increasing pressure or decreasing temperature because when the glass transition is reached further reductions in free volume are inhibited.

It was shown some time ago [2] that Eq. (1) generally fails to recover the greater than exponential pressure-viscosity behavior that is observed at high pressure. Now we shall investigate the accuracy of the temperature-viscosity behavior of Eq. (1) which has been used in so many thermal EHL analyses.

The mineral oil, LVI 260, was the subject of several investigations of thermal non-Newtonian behavior in concentrated contact [7–9]. The constitutive behavior was assumed to follow the Ree-Eyring law in these works, while the viscosity was assumed [8,9] to follow Eq. (1). The commonly held belief that the thermal regime of traction can be modeled in this way was to some extent established by the Johnson and Greenwood paper [9] using LVI 260.

Contributed by the Tribology Division of THE AMERICAN SOCIETY OF MECHANICAL ENGINEERS for presentation at the STLE/ASME Tribology Conference, Seattle, WA, October 1–4. Manuscript received by the Tribology Division Feb. 7, 2000; revised manuscript received June 27, 2000. Paper No. 2000-TRIB-25. Associate Editor: L. San Andrés.

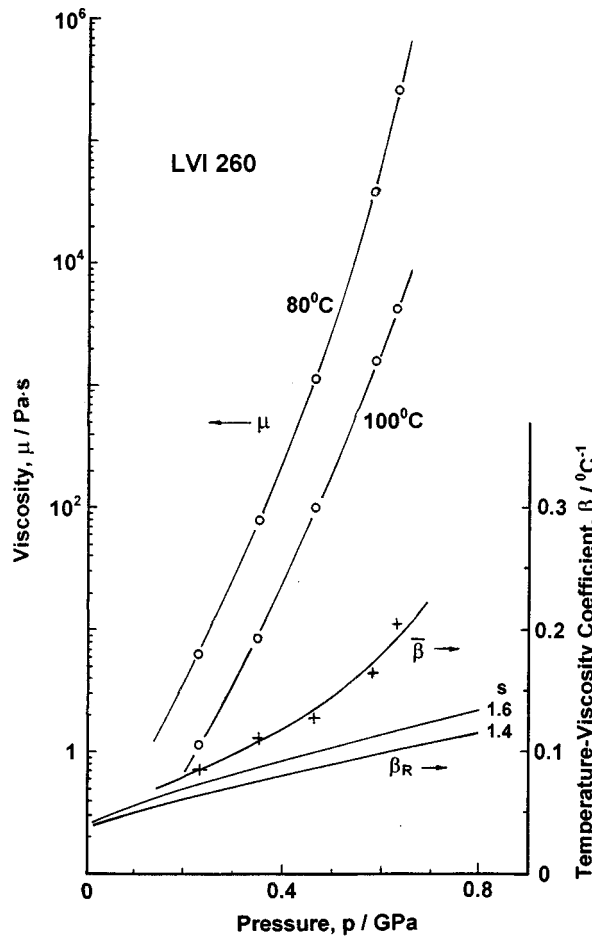


Fig. 1 Viscosity and temperature-viscosity coefficients for LVI 260. At 90°C, $\bar{\beta}$ is derived from the viscosity measurements shown and β_R is from Eq. (1) and the data of [8,9].

We have measured the viscosity of this mineral oil using a falling body viscometer and plotted the results for 80°C and 100°C versus pressure in Fig. 1. For the measured pressures, we have calculated a temperature-viscosity coefficient, $\bar{\beta}$, at 90°C from

$$\bar{\beta}(p) = \frac{\ln[\mu(80^\circ\text{C}, p) / \mu(100^\circ\text{C}, p)]}{100^\circ\text{C} - 80^\circ\text{C}} \quad (2)$$

These coefficients are plotted in Fig. 1.

Referring to Eq. (1), for $T_0 = 90^\circ\text{C}$, $\mu_0 = 0.017 \text{ Pa}\cdot\text{s}$ from Ref. [7], $z = 0.736$ from Ref. [8], and two values of s have been given, 1.4 in Ref. [8] and 1.6 in Ref. [9]. The usual temperature-viscosity coefficient,

$$\beta = \frac{-1}{\mu} \frac{\partial \mu}{\partial T} \quad (3)$$

can be obtained from the Roelands equation [9] as

$$\beta_R = s \ln(\mu(p) / \mu_R) / (T + 135^\circ\text{C}) \quad (4)$$

We have plotted β_R as curves for $s = 1.4$ and 1.6 in Fig. 1. At $p = 0.63 \text{ GPa}$ the Roelands equation already underestimates β by a factor of two. Note that in Ref. [8] pressures range to 1.4 GPa and in Ref. [9] the maximum pressure was 1.1 GPa . It is clear from Fig. 1 that the temperature-viscosity behavior of LVI 260 for $p > 1 \text{ GPa}$ is quite different from that which has been assumed for some investigations of thermal, non-Newtonian traction and the assumption of Eyring-Roelands behavior is questionable on the basis of just these data.

3 Viscosity Measurements of Real Lubricants

While it can be appreciated that the use of the Roelands equation for the representation of viscosity to high pressure is convenient for numerical work in that no singularity will be encountered with increasing pressure, progress toward realistic traction and micro-EHL modeling can only be made using the temperature-pressure-viscosity behavior of real lubricants. The following extensive viscosity measurements were performed using two falling body viscometers that have been described elsewhere [10,11].

The viscosity model utilized in this work is the pressure modified Williams, Landel, and Ferry equation introduced by Yasutomi et al. [12]. This model can reproduce the pressure-viscosity inflection, but only when that inflection is present in the regression data. In fact, it is necessary to have some viscosity data at pressures lower and higher than the inflection pressure to uniquely define all parameters. The viscosity is obtained from

$$\mu = \mu_g \exp\left[\frac{-2.3C_1(T - T_g)F}{C_2 + (T - T_g)F}\right] \quad (5)$$

where the glass transition temperature is

$$T_g = T_{g0} + A_1 \ln(1 + A_2 p) \quad (6)$$

and the relative free volume expansivity is

$$F = 1 - B_1 \ln(1 + B_2 p) \quad (7)$$

and A_1 , A_2 , B_1 , B_2 , C_1 , C_2 , and T_{g0} are parameters to be evaluated. Here μ_g and T_g are not necessarily the glass transition viscosity and temperature, but viscosity and temperature for an isoviscous reference state that parallels the glass transition. A derivation from free volume theory is available in Ref. [13]. Note that $\mu \rightarrow \infty$ as $T \rightarrow T_g - C_2/F$ where T_g and F are functions of pressure.

3.1 Automotive Transmission Fluids. Four liquid lubricants used in automobile transmissions were investigated at temperatures of 30°C, 70°C, and 120°C. They are listed in Table 1. The *M* and *D* fluids meet U.S. specifications and the *B* fluid is formulated to a European standard. The *H* fluid is used for a metal belt driven continuously variable transmission. The pressure-viscosity behavior among these fluids was similar. For example,

Table 1 Yasutomi parameters for transmission fluids. *M*: Mercon *D*: Dexron. *H*: Honda CVTF. *B*: Burmah.

Fluid	μ_g Pa·s	T_{g0} °C	A_1 °C	A_2 GPa ⁻¹	B_1	B_2 GPa ⁻¹	C_1	C_2 °C
<i>M</i>	10 ⁸	-105.9	143.4	0.7996	0.1688	26.41	12.44	44.65
<i>D</i>	10 ⁸	-99.21	156.0	0.7885	0.1784	25.11	12.56	44.39
<i>H</i>	10 ⁸	-98.74	171.1	0.7870	0.1781	26.02	12.64	43.97
<i>B</i>	10 ⁸	-110.1	133.1	0.8240	0.1557	27.90	12.62	47.02

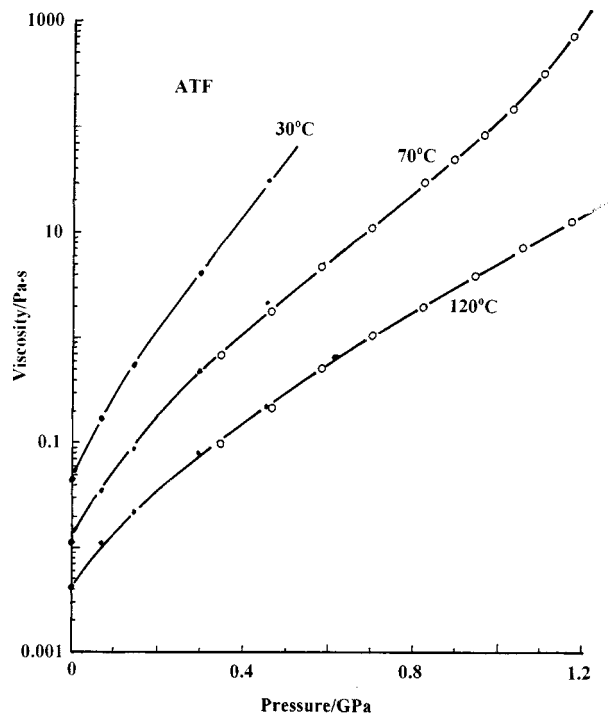


Fig. 2 The pressure-viscosity behavior of Mercon ATF

the viscosity of the *M* fluid is plotted against pressure in Fig. 2. Two different symbols are used to denote different viscometers. Note that the pressure-log viscosity inflection does not occur until the relatively high pressure of 0.8 GPa at 70°C, and that at 120°C the inflection had not been observed to 1.0 GPa. The Yasutomi parameters are listed in Table 1. The pressure-viscosity coefficient for calculating film thickness, α^* , is compared for the ATF fluids in Table 2. Note that α^* is the reciprocal of the asymptotic isoviscous pressure. See Table 3 for a comparison of viscosities at high pressure.

3.2 Aerospace Fluids. In Fig. 3 we have plotted the pressure-viscosity isotherms of a jet engine lubricant that meets specification Mil-L23699 for aircraft gas turbine engines. Temperature varies from 23°C to 165°C and pressure to 1.4 GPa. Note that the viscosity inflection can be observed in all isotherms except at 165°C. We expect that the inflection will occur at higher pressure for this temperature.

Table 2 Pressure-viscosity coefficient for transmission fluids α^*/GPa^{-1}

ATF	30°C	70°C	120°C
<i>M</i>	17.4	14.0	11.4
<i>D</i>	20.0	14.1	11.9
<i>H</i>	21.7	17.1	12.4
<i>B</i>	17.3	13.8	10.9

Table 3 Viscosity at $p=1.1$ GPa for transmission fluids, Pa·s

ATF	70°C	120°C
<i>M</i>	300	8
<i>D</i>	1000	27
<i>H</i>	4000	40
<i>B</i>	80	3.7

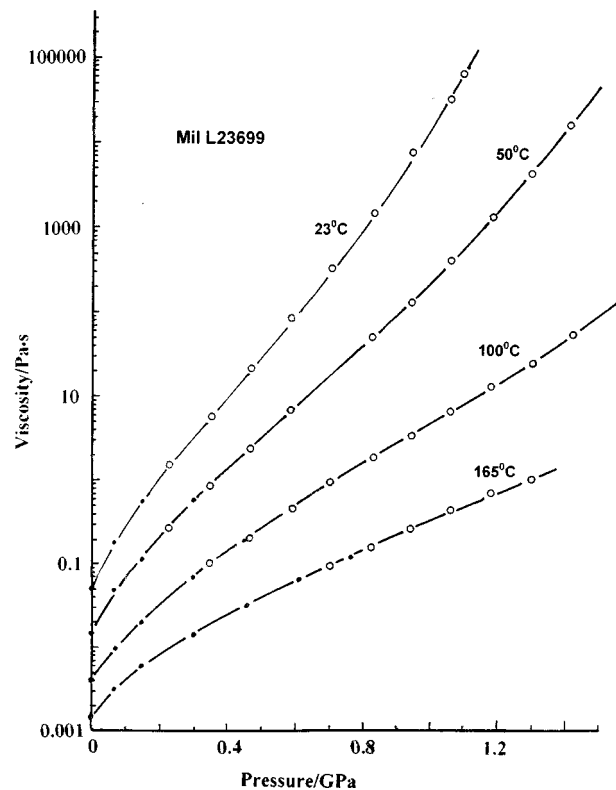


Fig. 3 Pressure-viscosity isotherms for a Jet II lubricant

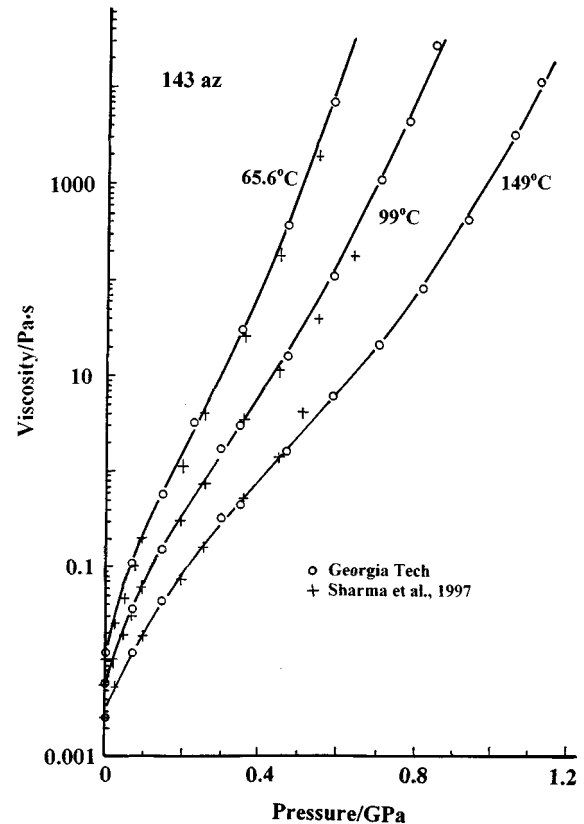


Fig. 4 Pressure-viscosity behavior of a fluorinated oil by two laboratories

Table 4 Yasutomi parameters for two aerospace fluids, a metal working oil, and a turbine oil

Fluid	μ_g Pa·s	T_{g0} °C	A_1 °C	A_2 GPa ⁻¹	B_1	B_2 GPa ⁻¹	C_1	C_2 °C
L23699	10 ¹²	-87.0	158	0.4476	0.194	18.8	16.03	22.52
134AZ	10 ¹²	-146.4	173.6	2.000	0.161	21.23	16.64	45.78
Somentor 31	10 ⁷	-131.0	28.87	11.49	0.270	13.12	11.13	20.13
T9	10 ⁷	-76.0	228.3	0.7645	0.188	25.84	11.45	30.26

Perfluorinated polyalkylethers are used for space applications and are being considered for the next generation of aircraft turbine lubricants. Isotherms are plotted in Fig. 4 for one of these branched fluorinated oils, 143 az. Data from another laboratory [14] is available and has been plotted in Fig. 4 as well. Agreement is good. Both laboratories observe the viscosity inflection at about 10 Pa·s. The Yasutomi parameters can be found for these fluids in Table 4.

3.3 Other Lubricants. Viscosity measurements were performed on a kerosene-based metal rolling oil, Somentor 31, for temperature to 80°C and pressure to 1.4 GPa. A mineral-based turbine oil, T9, was also tested to 100°C and 1.2 GPa. The Yasutomi parameters for these liquids are listed in Table 4.

4 Conclusion

Nearly all analyses of EHD traction and micro-EHD have utilized viscosity relations which underestimate the pressure-viscosity coefficient and the temperature-viscosity coefficient at high (>0.5 GPa) pressure. We present the parameters for real lubricants of a free volume viscosity relation which allows accurate calculation of viscosity for pressures approaching the glass transition. This relation predicts an unbounded viscosity at a pressure which increases with temperature. The use of averaged rheological properties is common for the analysis of concentrated contact traction. The averaged property must be obtained from integration over the contact area. Averaging techniques for which the contact pressure interval includes the viscosity singularity must therefore be suspect.

Acknowledgment

This work was supported by a grant from the Timken Company.

References

- [1] Bridgman, P. W., 1949, "Viscosities to 30,000 kg/cm², Especially Certain Liquids," *Proc. Am. Acad. Arts Sci.*, **77**, pp. 117–128.
- [2] Bair, S., 1993, "A Note on the Use of Roelands Equation to Describe Viscosity for EHD Hertzian Zone Calculations," *ASME J. Tribol.*, **115**, No. 2, p. 334.
- [3] Bair, S., 1999, "The Pressure-Viscosity Coefficient at Hertz Pressure and Its Relation to Concentrated Contact Traction," *Proc. 26th Leeds-Lyon Symposium on Tribology*, Rowson, et al., eds., Elsevier, Amsterdam.
- [4] Bondi, A., 1968, *Physical Properties of Molecular Crystals, Liquids and Glasses*, Wiley, New York, pp. 350–358.
- [5] Roelands, C., 1966, "Correlational Aspects of the Viscosity-Temperature-Pressure Relationship of Lubricating Oils," University Microfilms, Ann Arbor, MI.
- [6] Harrison, G., 1976, *The Dynamic Properties of Supercooled Liquids*, Academic Press, London, p. 28.
- [7] Conry, T. F., Johnson, K. L., and Owen, S., 1980, "Viscosity in the Thermal Regime of EHD Traction," Thermal Effects in Tribology, *Proc. 6th Leeds-Lyon Symposium on Tribology*, Dowson, D., Taylor, C. M., Godet, M. and Berthe, D., eds., Mech. Engr. Pub. Ltd., London, pp. 219–227.
- [8] Wang, S., Cusano, C., and Conry, T. F., 1991, "Thermal Analysis of Elastohydrodynamic Lubrication of Line Contacts Using the Ree-Eyring Fluid Model," *ASME J. Tribol.*, **132**, 2, pp. 232–244.
- [9] Johnson, K. L., and Greenwood, J. A., 1980, "Thermal Analysis of an Eyring Fluid in Elastohydrodynamic Traction," *Wear*, **61**, p. 367.
- [10] Bair, S., 1992, "An Experimental Verification of the Significance of the Reciprocal Asymptotic Isoviscous Pressure," *ASLE Tribol. Trans.*, **36**, No. 2, pp. 154 and 155.

- [11] Bair, S., 1999, "Pressure-Viscosity Behavior of Lubricants to 1.4 GPa and Its Relation to EHD Traction," STLE paper 99-TC-9, p. 5.
- [12] Yasutomi, S., Bair, S., and Winer, W., 1984, "An Application of a Free Volume Model to Lubricant Rheology," *Trans. ASME, J. Tribol.*, **106**, No. 2, pp. 291–303.
- [13] Bair, S., 1990, "High Shear Stress Rheology of Liquid Lubricants," Ph.D. thesis, Georgia Institute of Technology, pp. 30–32.
- [14] Sharma, S. K., Rosado, L., Hoglund, E., and Hamrock, B. J., 1995, "Rheology of Perfluoropolyalkylether Fluids in Elastohydrodynamic Lubrication," *STLE Tribol. Trans.*, **38**, No. 4, p. 772.

Numerical Contact Analysis of Transversely Isotropic Coatings: A Cylinder Within a Circumferential Groove

Clint Morrow, Michael Lovell,*
and Zhi Deng

Department of Mechanical Engineering, University of Pittsburgh, Pittsburgh, PA 15261

The contact characteristics of transversely isotropic coatings are investigated for a cylinder within a circumferential groove using a two-dimensional finite element model. With the model, contact behavior is evaluated at more than 400 operating conditions by varying coating material, coating thickness, normal load, and cylinder/groove radii. Based on the finite element results, numerical expressions are derived for the maximum surface pressure, contact length, and approach distance as a function of a transversely isotropic coating parameter, ζ . The importance of these expressions, as related to design and the selection of materials for reducing wear in contacting surfaces, is subsequently discussed. [DOI: 10.1115/1.1308008]

1 Introduction

Hard and soft surface coatings have gained substantial popularity over the past several decades for increasing the function life of contacting components. Despite their increased use, the selection of coating materials is often problematic for designers because current theoretical methods fail to successfully predict contact stress and deformation behavior in media that contain very thin (0.05–500 μm) anisotropic layers. Similar to other work in the literature [1–4], this paper utilizes the finite element method (FEM) to analyze the compliance behavior of coated surfaces. The specific geometry that will be investigated is a transversely isotropic coated cylinder that is in normal contact within a circumfer-

*Corresponding author

Contributed by the Tribology Division of THE AMERICAN SOCIETY OF MECHANICAL ENGINEERS for presentation at the STLE/ASME Tribology Conference, Seattle, WA, October 1–4. Manuscript received by the Tribology Division Feb. 2, 2000; revised manuscript received June 29, 2000. Paper No. 2000-TRIB-20. Associate Editor: T. C. Ovaert.

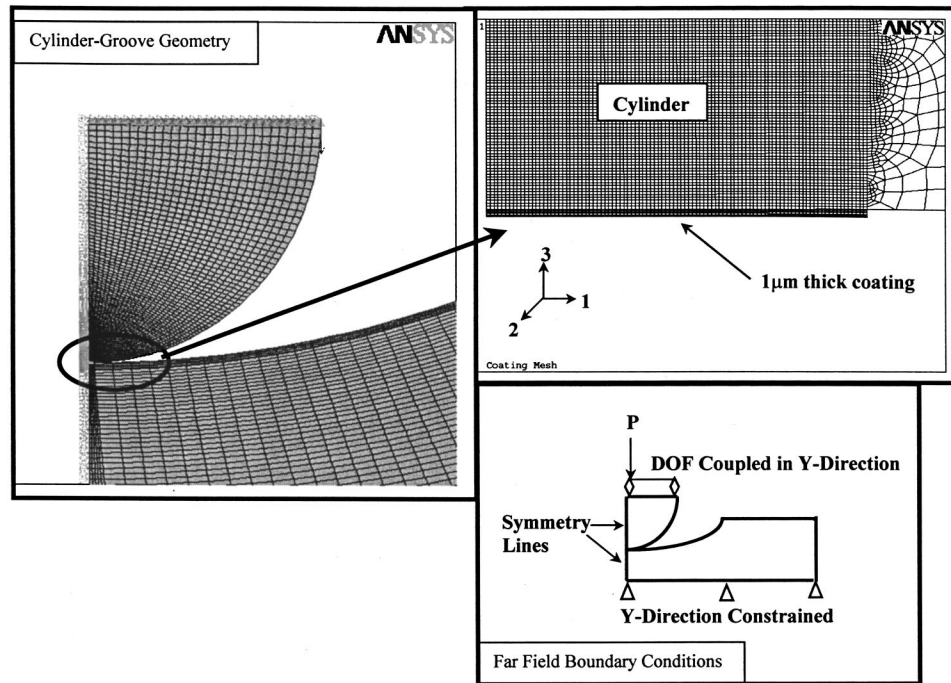


Fig. 1 Finite element model of cylinder in a circumferential groove

ential groove. By curve fitting the obtained FEM results, fundamental relationships for the maximum normal stress, contact length, and approach distance will be generated as a function of a dimensionless coating parameter, ζ [5].

$$\zeta = \frac{2PR_{\text{eff}}(1 + \nu_{12})E_{\text{cyl}}C_{33}C_{44}}{E_{\text{sub}}^4 t^2} \quad (1)$$

In Eq. (1), P is the normal load per unit length, E_{cyl} is the cylinder elastic modulus, R_{eff} is the effective cylinder-groove radius, ν_{12} , C_{33} , C_{44} , and t are the Poisson's ratio, normal elastic modulus, shear modulus, and thickness of the coating, and E_{sub} is the elastic modulus of the substrate. It is important to note that although ζ has no direct physical meaning, it incorporates the full transversely isotropic nature of the coatings. In particular, all five independent elastic constants (C_{11} , C_{12} , C_{13} , C_{33} , and C_{44}) are directly represented in the expression, as ν_{12} is defined by $C_{13}/(C_{11} + C_{12})$. As described in [5], ζ was established by taking the product of a dimensionless geometry/load (Go) parameter and a dimensionless material (Mo) parameter. Both of these parameters were obtained by performing an exhaustive search of the problem variables that yielded nondimensional quantities.

2 Finite Element Model

The finite element model used to generate stress, displacement, and approach distance results for a coated cylinder in normal contact within a circumferential groove was created using the commercial FEA code ANSYS 5.5®. As shown in Fig. 1, the model consisted of a rectangular grooved section that was in normal contact with a coated quarter cylinder. A sample mesh of the entire model is depicted in Fig. 1 along with the coating mesh and far field boundary conditions. It should be noted that due to the directionally dependent nature of the thin coatings analyzed, an extremely fine mesh was required in the region of contact to adequately capture gradients within the coating and discontinuities along the coating/substrate interface. Two-dimensional (plane stress), four-noded structural solid elements were used to define the cylinder and groove areas. Contact was defined between the groove-coating surfaces using three-noded point-to-surface con-

tact elements that utilize the penalty method. A typical model consists of 20,000 to 25,000 structural elements and 500 to 800 contact elements.

The boundary conditions applied to the finite element model are also depicted in Fig. 1. Symmetry was defined along the entire left-hand side of the cylinder and groove sections and the bottom horizontal edge of the grooved area were constrained in the vertical direction. At the top horizontal edge of the cylinder section, the nodal degrees of freedom were coupled in the vertical direction. Hence, when a point normal load was applied to the top of the cylinder, all of the nodes along the top surface were constrained to displace an equal amount in the vertical direction. The coatings were modeled to rigidly bond to the cylindrical substrate so that micro-structural boundary conditions were not incorporated for the coating. Table 1 lists the transversely isotropic soft and hard coatings analyzed in this work and their elastic constants. In the table, C_{11} corresponds to Young's modulus parallel to the substrate, C_{33} is the modulus perpendicular to substrate surface, and C_{44} is the shear modulus for the coating materials. The material properties for the elastic cylinder and groove substrates were held constant with the characteristics of steel ($E = 210$ GPa, $\nu = 0.29$).

As there are no known analytical or experimental results available for the geometry investigated, the accuracy of the FEM was

Table 1 Elastic constants for soft and hard coating materials (GPa)

Material	C_{11}	C_{33}	C_{44}	C_{12}	C_{13}	ν_{12}
MoS ₂ [6]	238	52	19	-54	23	0.125
NbSe ₂ [6]	106	54	19.5	14	31	0.258
Graphite [6]	1060	37	0.35	180	15	0.0121
InSe ₂ [6]	73	36	12	27	30	0.3
GaSe ₂ [6]	103	34	9	29	12	0.091
GaS [6]	157	36	8	33	15	0.079
Cadmium [7]	121	51.3	18.5	48.1	44.2	0.261
Cobalt [7]	307.0	358.1	75.3	165.0	103.0	.218
Al ₂ O ₃ [9]	460.2	509.5	126.9	174.7	127.4	.201
SiC [8]	479	521.4	148.4	97.8	55.3	.096

Table 2 Comparison of FEM results with Hertzian solutions

P (N/mm)	$R_{\text{eff}} 12.5 \text{ mm}$			$R_{\text{eff}} 33.3 \text{ mm}$		
	σ/σ_h	b/b_h	δ/δ_h	σ/σ_h	b/b_h	δ/δ_h
.5	1.029053	0.985072	1.023859	1.018094	0.987105	1.028935
.9	1.011647	0.971773	1.009597	1.019662	0.980993	1.02828
1.3	0.970071	1.047283	1.018924	1.016022	1.020294	1.027386
5.0	1.010473	1.02213	1.001885	1.023545	1.009895	1.024991
50	1.003827	1.038917	0.986204	0.996274	1.037894	1.017047

P (N/mm)	$R_{\text{eff}} 75 \text{ mm}$		
	σ/σ_h	b/b_h	δ/δ_h
.5	0.991436	0.995331	1.028794
.9	1.004798	1.011649	1.024844
1.3	0.98753	1.010091	1.028706
5.0	0.974027	1.00148	1.028018
50	0.966179	1.02246	1.022899

established by comparison to Hertzian contact theory. Following the approach used in [1,5,10,11], this was accomplished by replacing the coating material properties with that of the substrate in the finite element model. Table 2 contains the ratio of the finite element and Hertzian predicted results at 15 different conditions. The small difference between the Hertzian and FEM values indicates that the FEM does indeed generate accurate and reliable results.

3 Numerical Analysis

By varying the coating thickness, coating material, normal load, and cylinder radius, simulations were performed using the finite element model at 450 distinct operating conditions. These conditions included a variation of the following parameters:

- Coating thickness:* 0.1, 0.01, and 0.001 mm
- Coating material:* SiC, NbSe₂, graphite, Al₂O₃, cadmium, cobalt, GaS, GaSe₂, InSe₂, MoS₂
- Normal load:* 500, 900, 1300, 5000, and 50,000 N/m
- Coated cylinder radius:* 0.005, 0.010, 0.015 m
- Noncoated circumferential groove radius:* 0.025 m

In order to simplify the analysis of results obtained from the finite element simulations, all of the normal stress, contact length, and approach distance results were normalized with respect to the Hertzian values (denoted by subscript *h*). The normalized maximum normal stress, $\bar{\sigma}$, contact length, \bar{b} , and approach distance, $\bar{\delta}$, results are given below:

$$\bar{\sigma} = \frac{\sigma}{\sigma_h}, \quad \bar{b} = \frac{b}{b_h}, \quad \bar{\delta} = \frac{\delta}{\delta_h} \quad (2)$$

Once normalized, the normal contact stress, contact length, and approach distance were tabulated as a function of the dimensionless coating parameter, ζ , which is given in Eq. (1). In Eq. (1), R_{eff} is the effective radius of the cylinder in a circumferential groove:

$$R_{\text{eff}} = \frac{R_1 R_2}{R_1 - R_2} \quad (3)$$

where R_1 is the groove radius and R_2 is the cylinder radius. It should be noted that although Hertzian theory predicts that although the approach distance is infinite when two half-spaced are pressed together, we will consider the contact of a finite cylinder and groove for which [12] gives an approach distance expression.

4 Results and Discussion

In order to ascertain the Hertzian type expressions for a soft coated cylinder contacting a circumferential groove, the normalized normal stress, contact length, and approach distance values were plotted as a function of ζ as shown in Fig. 2. By curve fitting the plotted data, compliance relationships were obtained for the

conditions examined. Curve fitting of the numerical data was performed using the commercial software Origin 4.1, where the following relationships were determined:

$$\bar{\sigma} = \frac{-0.45666}{1 + (10.75153\zeta)^{0.45878}} + 0.99966 \quad (4)$$

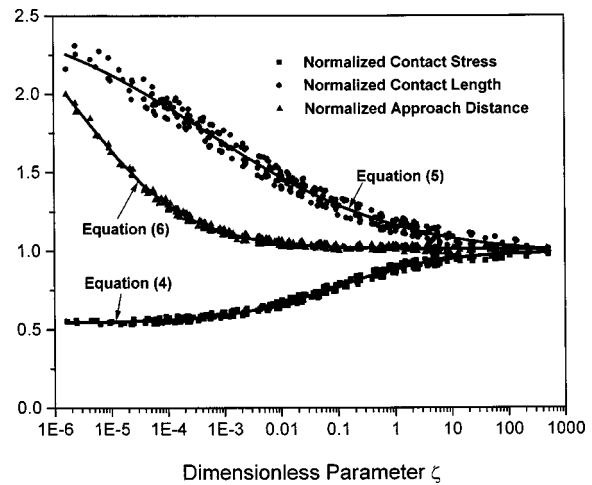


Fig. 2 Normalized soft coating results versus ζ

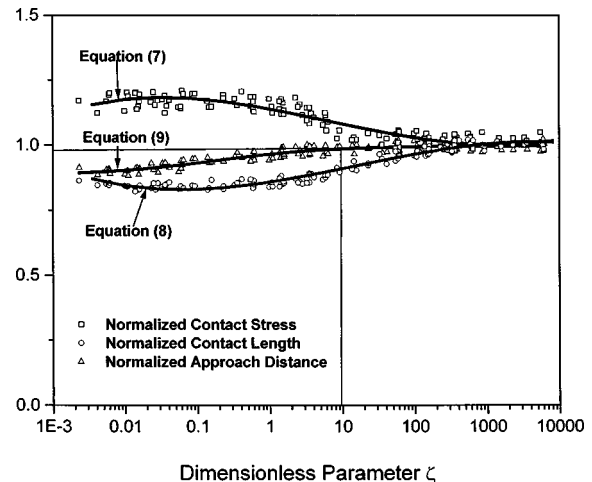
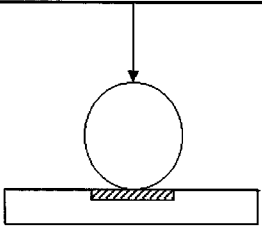
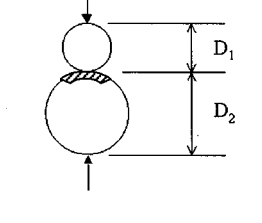
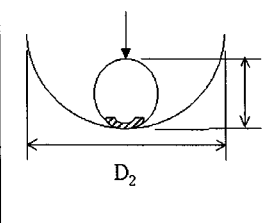


Fig. 3 Normalized hard coating results versus ζ

Table 3 Summary of numerical relationships developed for Hertzian geometries

Geometry	Soft Coating Expressions	Hard Coating Expressions
	$\bar{\sigma} = \frac{1.052}{1 + (47248\zeta)^{-0.1685}}$ $\bar{b} = \frac{1.26872}{(0.91203 + 0.01435 \ln \zeta)}$ $\bar{\delta} = \frac{0.1069}{1 + (370\zeta)^{-0.3532}} + 0.89478$	$\bar{\sigma} = 0.99464 + \frac{0.149}{1 + (7.3146\zeta)^{0.2574}}$ $\bar{b} = \frac{0.88072 + 19.865\zeta^{0.5}}{(1 + 1.22075\zeta^{0.5})}$ $\bar{\delta} = \frac{1.1122 + 19.865\zeta^{0.5} + 3.701\zeta}{1 + 19.714\zeta^{0.5} + 3.7012\zeta}$
	$\bar{\sigma} = \frac{-0.52675}{1 + (36.44315\zeta)^{0.44976}} + 0.98261$ $\bar{b} = \frac{1.26872}{1 + (132.97872\zeta)^{0.4656}} + 1.02091$ $\bar{\delta} = \frac{0.83247}{1 + (1155.04117\zeta)^{0.55324}} + 1.00178$	$\bar{\sigma} = \frac{0.16425}{1 + (0.10719\zeta)^{1.02371}} + 1.01861$ $\bar{b} = \frac{-0.1863}{1 + (0.56209\zeta)^{0.43854}} + 1.00884$ $\bar{\delta} = \frac{-0.10921}{1 + (3.06626\zeta)^{0.58374}} + 0.99930$
	$\bar{\sigma} = \frac{-0.45666}{1 + (10.75153\zeta)^{0.45878}} + 0.99966$ $\bar{b} = \frac{1.68267}{1 + (2818.18745\zeta)^{0.24076}} + 0.95063$ $\bar{\delta} = \frac{1.77039}{1 + (357104.5959\zeta)^{0.46216}} + 1.01044$	$\bar{\sigma} = \frac{0.1481}{1 + (0.16565\zeta)^{1.92668}} + 1.01854$ $\bar{b} = \frac{-0.16526}{1 + (0.054505\zeta)^{0.78575}} + 1.00892$ $\bar{\delta} = \frac{-0.11523}{1 + (4.24178\zeta)^{0.55849}} + 0.9998$

$$\bar{b} = \frac{1.68267}{1 + (2818.18745\zeta)^{0.24076}} + 0.95063 \quad (5)$$

$$\bar{\delta} = \frac{1.77039}{1 + (357104.5959\zeta)^{0.46216}} + 1.01044 \quad (6)$$

As shown by the function lines in Fig. 2, Origin provided an accurate fit of the three sets of data. The χ -squared values for Eqs. (4)–(6) were 4.85×10^{-3} , 4.00×10^{-3} , and 13.92×10^{-3} , respectively.

Similar to the soft coatings, the hard coating results depicted in Fig. 3 were found to be a continuous function of ζ . Utilizing Origin 4.1, the following relationships were determined:

$$\bar{\sigma} = \frac{0.1481}{1 + (0.16565\zeta)^{1.92668}} + 1.01854 \quad (7)$$

$$\bar{b} = \frac{-0.16526}{1 + (0.054505\zeta)^{0.78575}} + 1.00892 \quad (8)$$

$$\bar{\delta} = \frac{-0.11523}{1 + (4.24178\zeta)^{0.55849}} + 0.9998 \quad (9)$$

The quality of the curve fitting is denoted by the small χ -square values of 2.66×10^{-4} , 2.16×10^{-4} , and 4.18×10^{-5} for the normalized contact stress, contact length, and approach distance, respectively. It is important to mention that the determined expressions (4)–(9) should only be considered valid over the range of parameters examined in this work. Two particular cases for which extrapolation should not be performed are for a rigid cylinder and for a geometry with a large effective radius. For a rigid cylinder, ζ approaches infinity, and the normalized Hertzian expressions become constant. For cases of large effective radius values ($R_{\text{eff}} \geq 0.015$ m), preliminary numerical results did not exhibit a continuous trend with ζ . Such a finding can be explained by the fact that Hertzian theory breaks down for large lines of contact, as pointed out by Ugural and Fenster [13].

In addition to developing expressions for coated surfaces, a second objective of this paper is to illustrate the usefulness of Eqs. (4)–(9). To this end, we will consider the problem of a 0.01 m radius cylindrical roller bearing element that is in a 0.025 m radius groove. Both the cylinder and groove are made of steel ($E = 207$ GPa and $\nu = 0.3$). If the cylindrical bearing element is subjected to a maximum normal load of 5000 N/m, we determine the required coating thickness of Al_2O_3 that must be applied to ensure that the centerline vertical displacement of the cylinder will not exceed $0.2 \mu\text{m}$. For the sample conditions, the ratio of the maximum allowable displacement to the predicted Hertzian value is 0.985. To solve the problem posed, one would simply determine the abscissa value that corresponds to an ordinate value of 0.985 on the approach distance curve of Fig. 3. For this case, an abscissa value of $\zeta = 9.32$ is found, which can be directly substituted into Eq. (1) to determine an Al_2O_3 coating thickness of $12.242 \mu\text{m}$.

5 Summary and Conclusions

In this paper, coated contact relationships were generated for the geometry of an elastic cylinder within a circumferential groove. These relationships represent the final contribution of an effort to obtain transversely isotropic coating expressions for the three basic Hertzian contact geometries. The geometries of a cylinder on a plane and two cylinders in contact were, respectively, examined in [5,10], and [11]. The results of these efforts, in combination with the results of this work, are summarized in Table 3. All of the expressions given in Table 3 were established to provide a useful reference for designers and analysts to evaluate the potential benefits of thin transversely isotropic coatings.

References

- [1] Gupta, P. K., and Walowit, J. A., 1990, "Modeling of Stresses In Coated Solids," SBIR Program Report No. F33615-89-C-5648, pp. 1–65.
- [2] Tian, H., and Saka, N., 1991, "Finite Element Analysis of an Elastic-Plastic Two-Layered Half Space: Sliding Contact," *Wear*, **148**, pp. 261–285.
- [3] Kral, E. R., and Komvopoulos, K., 1996, "Three Dimensional Finite Element

- Analysis of Subsurface Stresses and Shakedown Due to Repeated Sliding on a Layered Elastic Medium," ASME J. Appl. Mech., **63**, pp. 967–973.
- [4] Kral, E. R., and Komvopoulos, K., 1997, "Three Dimensional Finite Element Analysis of Subsurface Stress and Strain Fields Due to Sliding Contact on an Elastic-Plastic Layered Medium," ASME J. Tribol., **119**, pp. 332–341.
- [5] Lovell, M. R., 1998, "Analysis of Contact Between Transversely Isotropic Coated Surfaces: Development of Stress and Displacement Relationships Using FEM," Wear, **214**, pp. 165–174.
- [6] Gardos, M., 1990, "On the Elastic Constants of Thin Solid Lubricant Films," *Mechanics of Coatings*, Elsevier, Amsterdam, The Netherlands, pp. 3–13.
- [7] Kuo, C. H., and Keer, L. M., 1992, "Contact Stress Analysis of a Layered Transversely Isotropic Half Space," ASME J. Tribol., **114**, pp. 253–262.
- [8] Martin, R. M., 1972, "Relation Between Elastic Tensors of Wurtzite and Zinc-Blende Structure Materials," Phys. Rev. B, **6**, pp. 4546–4553.
- [9] Gieske, J. H., and Barsch, G. R., 1968, "Pressure Dependence of the Elastic Constant of a Single Crystalline Aluminum," Phys. Status Solidi, **29**, pp. 121–131.
- [10] Lovell, M. R., 1999, "Determination of Compliance Relationships for Transversely Isotropic Hard Surface Coatings Using the Finite Element Method," ASME J. Tribol., **121**, pp. 416–418.
- [11] Morrow, C., and Lovell, M., 1999, "Numerical Contact Analysis of Transversely Isotropic Coated Cylinder," to appear in Wear.
- [12] Roark, R. J., and Young, W. C., 1975, *Formulas for Stress and Strain*, McGraw-Hill, New York, p. 517.
- [13] Ugural, A. C., and Fenster, S. K., 1994, *Advanced Strength and Applied Elasticity*, Prentice-Hall, Englewood Cliffs, NJ, pp. 133–135.